Analytica Chimica Acta 1166 (2021) 338547

Contents lists available at ScienceDirect

Analytica Chimica Acta

journal homepage: www.elsevier.com/locate/aca

# Zwitterions for impedance spectroscopy: The new buffers in town

Satyam Anand [1], Pragya Swami [1], Gaurav Goel **, Shalini Gupta *

*Dept. of Chemical Engineering, Indian Institute of Technology Delhi, New Delhi, 110016, India*

## HIGHLIGHTS

- Good's zwitterionic buffers show improved performance in impedance spectroscopy measurements of bacterial suspensions.
- Higher ion-ion interactions in zwitterionic buffers lead to lower conductivities and enhanced impedance sensing ability.
- Increased sensitivity for impedance measurements in zwitterionic buffers illustrated using *S. typhi* and *S. aureus* bacteria.

## GRAPHICAL ABSTRACT

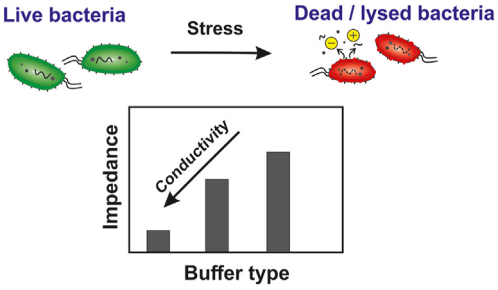


## ARTICLE INFO

*Article history:*
Received 25 November 2020
Received in revised form
3 April 2021
Accepted 5 April 2021
Available online 24 April 2021

*Keywords:*
Zwitterion
Impedance
Biosensor
Bacteria

## ABSTRACT

Studying the role of buffers in impedance spectroscopy is a relatively unexplored area. We demonstrate a special class of biologically relevant buffers known as Good's zwitterionic buffers that show improved performance over standard electrolyte buffers (*e.g.* PBS) currently widely used in impedance spectroscopy measurements of bacterial suspensions. Our theoretical and experimental comparisons of conductivity of classical and zwitterionic buffers at various different concentrations show that ion-ion interaction effects are significantly higher in zwitterionic buffers as compared to classical buffers at the concentrations at which they are used. This and the fact that zwitterions have larger sizes leads to the lowering of their conductivity which significantly improves their impedance sensing ability. We illustrate through an example of heat-induced ionic release in model *S. typhi* and *S. aureus* bacteria that having a low conductivity buffer is indeed beneficial for biological impedance measurements. In fact, the best buffer for impedance studies can be chosen solely based on their electrical properties as long as they are also biologically compatible. This gives Good's zwitterionic buffers an edge over conventional media as they satisfy both these criteria.



## 1. Introduction

Impedance spectroscopy is a simple and label-free tool for high-throughput analyses of bacteria and bacteria-related events in real-time [1–3]. Its common applications for bacterial sensing include:

I. Tracking microbial growth by measuring changes in impedance response due to increase in biomass (direct approach). This requires the use of growth buffers [4].
II. Monitoring cellular activity or survival by measuring changes in medium conductivity due to release of cell metabolites, ions *etc.* (indirect approach). This typically takes place in response to an external stimulus (*e.g.* antibiotics) and requires standard buffers or DI water [5].

* Corresponding author.
** Corresponding author.
*E-mail addresses:* goelg@chemical.iitd.ac.in (G. Goel), shalinig@chemical.iitd.ac.in (S. Gupta).
[1] Equal contribution.

https://doi.org/10.1016/j.aca.2021.338547
0003-2670/

III. Measuring changes in blockade current as cells get immobilized on a pre-functionalized electrode surface (direct approach) [6,7]. This requires use of buffers since the immobilization step typically involves biological interactions.

Traditionally, impedance measurements of biological systems are performed in phosphate buffer saline (PBS), tris-HCl buffer, growth media, glucose, mannitol, or deionized (DI) water [8–13]. While DI water provides the lowest background conductivity (favorable for impedance measurements), it also has an unstable pH and induces a large osmotic pressure on the cells. 1x PBS, on the other hand, provides an ideal isotonic environment with good buffering capacity that improves cell survival near the physiological pH. In spite of this, 1x PBS is not the best choice of medium for carrying out impedance studies due to its high conductivity (~1.68 S/m). As a result, many impedance experiments are performed after diluting the PBS 100 to 1000 times [14–17]. This, however, makes the medium hypotonic and reduces its buffering capacity, putting undue stress on the cells as in the case of DI water.

The current trends in impedance biosensors all focus on electrode design and cell enrichment strategies to improve signal sensitivity and limits of detection [18–22]. There is very little emphasis on the use of novel buffers to enhance detection sensitivity [23,24], defined here as the relative impedance change in osmotic pressure-matched buffers. In general, it is well known that a low conductivity medium gives rise to a large value of absolute impedance, as evident from the inverse relationship between complex conductivity ($\tilde{K}(\omega)$) and impedance ($\tilde{Z}(\omega)$) (eq. (1)),

$$\tilde{Z}(\omega) = \frac{C_c}{\tilde{K}(\omega)} \tag{1}$$

Here, $C_c$ is the system's geometrical cell constant and $\omega$ is the angular frequency. A large impedance value inevitably means a high signal but there is also a possibility of higher background noise in low conductivity media, forcing one to perform experiments in an "appropriate" low conductivity buffer that has higher impedance signal coupled with low background noise, leading to more sensitive biosensing [25].

What is perhaps less obvious is that a low conductivity medium also gives rise to a higher *change in impedance* which can then be utilized for reporting the data more sensitively. Given that $\tilde{K}(\omega)$ and $\tilde{Z}(\omega)$ are, respectively, the conductivity and impedance of the medium alone, and $\tilde{K}(\omega) + \Delta\tilde{K}(\omega)$ and $\tilde{Z}(\omega) + \Delta\tilde{Z}(\omega)$ are the conductivity and impedance after the addition of cells to this medium, using eq. (1) we get,

$$\Delta\tilde{Z}(\omega) = \frac{C_c}{\tilde{K}(\omega) + \Delta\tilde{K}(\omega)} - \frac{C_c}{\tilde{K}(\omega)} \tag{2}$$

This is a complex equation where both the real and imaginary parts of $\tilde{K}(\omega)$ and $\Delta\tilde{K}(\omega)$ can contain frequency-dependent terms. For impedance measurements in which the real parts dominate the imaginary parts, we can safely neglect the imaginary parts and get a simplified relationship (eq. (3)) in terms of $K'(\omega)$ or $\kappa$ (real component of $\tilde{K}(\omega)$, also known as DC or ohmic conductivity) (discussed later in section 2.2). This approximation holds true for most cases and especially those pertaining to solution conductivity changes during cellular ionic release.

$$\Delta Z = \frac{C_c}{\kappa + \Delta\kappa} - \frac{C_c}{\kappa} = \frac{-\Delta\kappa . C_c}{\kappa . (\kappa + \Delta\kappa)} \tag{3}$$

Here it can be seen that between any two systems having the same $\Delta\kappa$ value (i.e., the same number of cells), the one with a lower $\kappa$ value translates to a higher $\Delta Z$ response, and in turn, better detection. In other words, compared to a high conductivity medium, cells suspended in a lower conductivity medium contribute more to the overall change in impedance response relative to the ionic species already present in the background. Therefore, it appears wiser to report impedance results in terms of differential impedance [19,26–28] rather than absolute values as done in many papers. Subtracting impedance comes with its own limitations though, as additional correction terms may be required below threshold frequencies due to electrode polarization artifacts [29].

There are additional benefits of using low conductivity media for cell impedance studies. One, they allow more electric field to penetrate through the cells at relatively lower frequencies. This helps in studying individual cell properties in greater detail, ensuring complete characterization of different cell components, viz. wall, membrane, and cytoplasm. Second, low conductivity media also enhance electrokinetic forces (in particular, positive dielectrophoretic force) leading to greater cell enrichment near the electrode surface, thereby enhancing biosensor sensitivity. Third, having less number of total ions present in the medium tends to minimize Joule heating and electrolytic effects that can lead to larger temperature variation and water splitting in miniaturized sample volumes.

The widely popular low conductivity media such as DI water or diluted PBS are excellent for monitoring metabolic activity or ionic release of cells for detection purposes, but fare rather poorly for carrying out cell viability studies (in the absence/presence of external stimulus) as they give faulty baselines due to unwarranted ionic release by cells under stress due to hypotonicity. Good's zwitterionic molecules are a special class of buffers that are extensively used in biological and biochemical research. They are water soluble, have $pK_a$ values between 6 and 8 (with minimal dependence on temperature, ionic strength and concentration) and are impermeable to cell membranes, which makes them an ideal medium for living cells [30–32]. Additionally, these buffers have surprisingly low conductivities at the concentrations at which they are used (typically 15–40 mM). For example, 15 mM of 4-(2-hydroxyethyl)-1-piperazineethanesulfonic acid (HEPES) buffer at pH 7.4 has a conductivity of only 0.04 S/m which is more than 40x lower than that of 1x PBS.

In the literature, very few impedance studies report the use of zwitterionic buffers. Our own studies with HEPES, however, show it to be a more sensitive medium than PBS for particle detection and bacterial cell viability analyses [27,33]. Clearly, everything else remaining same, these low conductivity Good's buffers provide a viable alternative as a medium for probing live cell impedance. In this article, we investigate both theoretically and experimentally the role of zwitterionic electrolytes in enhancing the sensitivity of impedance signals of bacterial suspensions.

## 2. Theoretical analysis of electrolytes in aqueous media

In order to quantitatively study the electrical properties of an electrolyte in aqueous medium, we introduce the term complex dielectric permittivity ($\tilde{\varepsilon}$) which can be related to complex conductivity and impedance as discussed below.

$$\tilde{\varepsilon}(\omega) = \varepsilon'(\omega) - i\varepsilon''(\omega) \tag{4}$$

In eq. (4). $\varepsilon'(\omega)$ and $-\varepsilon''(\omega)$ denote the real and imaginary parts of permittivity, respectively. Similarly, complex conductivity can be expanded into its real ($K'(\omega)$ or $\kappa$), and imaginary ($K''(\omega)$) components using eq. (5),

$$\tilde{K}(\omega) = K'(\omega) + iK''(\omega) \quad (5)$$

By definition, complex permittivity and complex conductivity are related to each other as depicted in eq. (6),

$$\tilde{K}(\omega) = i\omega\tilde{\varepsilon}(\omega) \quad (6)$$

By combining eqs. (4) to (6), we obtain eqs. (7) & (8),

$$\varepsilon'(\omega) = \frac{K''(\omega)}{\omega} \quad (7)$$

$$\varepsilon''(\omega) = \frac{\kappa}{\omega} \quad (8)$$

The real part of dielectric permittivity represents the energy storage term and is a measure of the system's overall polarizability. In “classical electrolytes”, the main contribution to energy storage comes from the dipolar water molecules, whereas in non-classical electrolytes such as zwitterions, the contributions result from both water and net neutral zwitterionic molecules. Analogously, the real part of conductivity (also called the ohmic or DC conductivity) signifies dissipation arising from the physical displacement of ions in the presence of an external electric field.

We can relate the modulus of experimentally measured impedance ($\left|\tilde{Z}(\omega)\right|$) to more fundamental properties like conductivity and permittivity by using a similar expansion for $\tilde{Z}(\omega)$ (eq. (9)),

$$\tilde{Z}(\omega) = Z'(\omega) + iZ''(\omega) \quad (9)$$

Combining eqs. (1), (5), (7), and (9), we get eq. (10),

$$\left|\tilde{Z}(\omega)\right| = \frac{C_c}{\sqrt{\kappa^2 + (\omega.\varepsilon'(\omega))^2}} \quad (10)$$

in which we can clearly see that $\left|\tilde{Z}(\omega)\right|$ can be increased by decreasing either the DC conductivity ($\kappa$) or the product of $\omega$ and $\varepsilon'$. We now investigate both these terms in greater detail below.

### 2.1. Ionic conductivity of electrolytes

An electrolyte dissociates into its corresponding ions when it is added to water. The dissociation can be complete or incomplete depending upon whether the electrolyte is weak or strong. The dissociated ions are hydrated by water molecules (in fact, hydration is the main thermodynamic force behind dissociation [34]) and the extent of hydration can vary between different ions depending on their size, structure, and charge.

When an electric field is applied across an aqueous electrolyte, ions move to the oppositely charged electrodes. This physical movement of ions constitutes the conductivity of this electrolyte solution. The overall conductivity can be written as a sum of the individual conductivity contributions from all the cations and anions present in the system as shown in eq. (11),

$$\kappa = \kappa_+ + \kappa_- = \lambda_+ C_+ + \lambda_- C_- \quad (11)$$

where, $\lambda_+$ and $\lambda_-$ are the molar conductivities of the cation and anion, respectively, $C_+$ and $C_-$ are the cation and anion molar concentrations in solution, respectively (can be different from the overall electrolyte concentration ($C_{el}$) added). Molar conductivity of a solution is defined as (eq. (12)),

$$\Lambda = \frac{\kappa}{C_{el}} \quad (12)$$

One mole of strong electrolyte $A_xB_y$ completely dissociates into $x$ stoichiometrically equivalent moles of $A^{y+}$ (aq) and $y$ moles of $B^{x-}$ (aq). Accordingly, we can write $C_+ = x.C_{el}$ and $C_- = y.C_{el}$. Using this relation along with eqs. (11) and (12), we obtain (eq. (13)),

$$\Lambda = x\lambda_+ + y\lambda_- \quad (13)$$

As $C_{el} \to 0$, $\Lambda$ approaches $\Lambda^0$, also known as the limiting molar conductivity. Eq. (13) can then be rewritten as,

$$\Lambda^0 = x\lambda_+^0 + y\lambda_-^0 \quad (14)$$

Eq. (14) is also known as the Kohlrausch's law of independent migration and is widely used to calculate the limiting molar conductivities of electrolytes using tabulated limiting conductivities of their individual ions ($\lambda^0$). Eq. (14) can be used to calculate conductivity of an electrolyte under very dilute/ideal conditions, where no ion-ion interactions exist ($\Lambda = \Lambda^0$). In practice, however, non-ideality often comes into play at the working concentrations of almost all electrolytes, which makes $\Lambda$ a concentration-dependent parameter. For strong electrolytes, it is experimentally found that (eq. (15)),

$$\Lambda = \Lambda^0 - \text{constant}\sqrt{C_{el}} \quad (15)$$

The deviation in $\Lambda$ from $\Lambda^0$ arises due to many reasons like ionic cloud relaxation and electrophoretic effects [35]. Debye-Hückel-Onsager gave a detailed understanding of this phenomenon in 1927 [36,37] and came up with a theoretical equation (eq. (16)) (for a 1:1 strong electrolyte) reminiscent of the empirical eq. (15).

$$\Lambda_{\text{theo.}} = \Lambda^0 - S\sqrt{C_{\text{actual}}} \quad (16)$$

Here, $S = a + b\Lambda^0$ where $a$ and $b$ are constants that depend on temperature, permittivity, and viscosity of the solution [35]. An important thing to note here is that in eq. (16), $C_{\text{actual}}$ is the actual amount of electrolyte available in solution (the portion that dissociates), whereas, in eq. (15), $C_{el}$ is the total electrolyte concentration added to the solution. As we move to higher concentrations, ions begin to associate and $C_{\text{actual}}$ becomes less than $C_{el}$ giving a deviation from eq. (15). As we shall see in the subsequent sections, this plays a role in the zwitterionic conductivity, as ionic conductivity, $\kappa$, becomes the most important, in fact the only parameter that directly affects $\left|\tilde{Z}(\omega)\right|$ in eq. (10).

### 2.2. Dielectric permittivity of electrolytes

The frequency dependence of dielectric permittivity comes from the fact that electric dipoles cannot change their orientation instantaneously in response to an externally applied electric field. In other words, there is a time lag associated with the change in dipolar orientation. The relaxation frequency for water dipoles is rather high (in GHz) whereas, impedance measurements for biological entities are performed below 50 MHz. Therefore, $\varepsilon'(\omega)$ of water can be considered independent of $\omega$ for all practical purposes. $\varepsilon'(\omega)$ can also be expressed in terms of relative permittivity ($\varepsilon_r$) as $\varepsilon_r = \frac{\varepsilon'(\omega)}{\varepsilon_0}$, where $\varepsilon_0$ is the permittivity of vacuum. The value of $\varepsilon_r$ for water is ~80 at 20°C.

When an electrolyte is added to water, the relative permittivity of the medium falls. This happens due to two reasons. First, the dipolar water molecules are replaced by isotropic ions, leading to a

reduction in the number of dipolar species present per unit volume [38]. Secondly, the water molecules trapped in the hydration shell around the ions lose their orientational mobility. Since these water molecules are under the influence of an additional local ionic field, they cannot move freely in response to the externally applied electric field. This results in "dielectric decrement" which can be quantitatively written as shown in eq. (17),

$$\varepsilon_s = \varepsilon_w + \delta.C_{el} \tag{17}$$

Here, $\varepsilon_s$ and $\varepsilon_w$ are the relative permittivities of the electrolyte solution and pure water respectively, and $\delta$ is a phenomenological constant ($M^{-1}$). The value of $\delta$ for a typical electrolyte (*e.g.* NaCl) is around $-11\ M^{-1}$[39]. Therefore, for 1x PBS, which can be simply approximated as 151.6 mM NaCl, $\varepsilon_s$ is estimated to be 78.3.

The addition of neutral dipolar molecules, instead of simple ionic electrolytes, affects the relative permittivity of the solution very differently. Neutral dipolar molecules like HEPES, in their zwitterionic form, possess a high dipole moment (23.8 D as compared to 1.85 D of water) due to the large separation between their positive and negative charge centers [40]. These molecules have larger polarizability compared to an equivalent volume of bulk water. This leads to an increase in its permittivity. Like the dielectric decrement in the case of ions, this increment can also be quantitatively approximated by eq. (17).

The fraction of neutral (or conversely anionic) molecules in a 20 mM HEPES solution at pH 7.4 can be calculated using the Henderson-Hasselbalch equation (eq. (18)),

$$pH = pK_a + \log_{10}\frac{[A^-]}{[HA]} \tag{18}$$

The $pKa_2$ value of HEPES is equal to 7.5 [32]. Therefore, at a pH of value 7.4, which is close to $pKa_2$, we get $[A^-] \approx [HA]$, which means that half of the HEPES molecules in solution exist in the neutral form and the other half as anions. As a result, the $\delta.C_{el}$ term in eq. (17) in case of HEPES can be represented by two separate parts, one capturing the dielectric increment due to its neutral form and the other as dielectric decrement due to anions. Since $[A^-] \approx [HA]$, $C_{el}$ becomes 10 mM for both parts. Further, $\delta$ due to neutral molecules is reported to be around 90 $M^{-1}$ for HEPES [41], and we take $\delta$ due to dissociated HEPES to be $-11\ M^{-1}$ (same as that of NaCl as $\delta$ for $Na^+HEPES^-$ is not reported in literature and typical $\delta$ values for 1:1 strong electrolytes lie in the range of $-8$ to $-15\ M^{-1}$) [39]. The net effect of both these factors turns out to be a dielectric increment of 0.79, which is non-appreciable.

Further, if we look at eq. (10), a high value of impedance depends not only on $\varepsilon'(\omega)$ but the product $\omega\varepsilon'(\omega)$. Since the practical frequency range for performing impedance measurements in biological samples is 10 Hz–100 kHz, putting $\varepsilon' = 80\varepsilon_0$ and $f = 100$ kHz yields $\omega.\varepsilon'(\omega) = 2\pi f.\varepsilon'(\omega) = 4.4 \times 10^{-4}$ $S.m^{-1}$. On comparing this product to $\kappa$, which has a typical value of 0.01–1 $S.m^{-1}$, we see that it can easily be ignored with respect to $\kappa$ unless one works at very high frequencies (GHz range). This was essential to establish because it rules out the effect of change in dielectric constant as a potential reason for unusually high impedance readings observed in zwitterionic buffers.

## 3. Experimental analysis of electrolytes in aqueous media

### 3.1. Comparison of ideal versus experimental conductivity behaviour

We compared the conductivities of HEPES and PBS buffers at different concentrations. Calculation of $\kappa_{ideal}$ (at infinite dilution) for 1x PBS at pH 7.4 having a composition of 137 mM NaCl, 2.7 mM KCl, 10 mM $Na_2HPO_4$, and 1.8 mM $KH_2PO_4$ yielded a total $Na^+$ concentration of 151.6 mM and a total $Cl^-$ concentration of 142 mM (other ions being much less in concentration were safely neglected). By taking PBS to be equivalent to 151.6 mM NaCl in order to simplify our calculations and putting values in eq. (14), we obtained $\Lambda^0 = \lambda^0_{Na^+} + \lambda^0_{Cl^-} = 0.0126$ $S.m^2.mol^{-1}$ and $\kappa_{ideal} = \Lambda^0.C_{el} = 1.91$ $S.m^{-1}$. Similarly, $\kappa_{ideal}$ for 20 mM HEPES at pH 7.4 having composition of 10 mM $HEPES^-$ and 10 mM neutral zwitterions was calculated as $\Lambda^0 = \lambda^0_{Na^+} + \lambda^0_{HEPES^-} = 0.0072$ $S.m^2.mol^{-1}$ and $\kappa_{ideal} = \Lambda^0.C_{el} = 0.072$ $S.m^{-1}$ [42,43].

The comparison between ideal and experimental values of PBS conductivity at different concentrations is shown in Table 1. We found that PBS does not show much deviation from ideal behaviour even at relatively high electrolyte concentrations of 151.6 mM, meaning that ion-ion interactions are still very weak at this concentration. HEPES, on the other hand, showed a significant deviation from its ideal behaviour even at a low concentration of 15 mM (the actual HEPES electrolyte concentration was only 7.5 mM) (Table 2). A possible reason for reduced conductivity in HEPES was initially contemplated to be associated with the lowering of $C_{actual}$ value which can occur due to ionic association in highly concentrated electrolytes [35] or electrolytes in confined spaces [44] as reported for ionic liquids [45,46]. Both these reasons were, however, ruled out as they did not apply to our system.

To further look into the possibility of anion ($HEPES^-$) and/or zwitterion (HEPES) molecular interaction, we compared the deviation from ideality in two cases: one where 50% molecules existed in the neutral form ($pH = pKa_2$) versus one where essentially no neutral molecules were present ($pH = pKa_2 + 1$, see eq. (18)). The percentage deviation from ideality in both cases was found to be very similar (~30% as shown in Table 2), leading us to conclude that ion/zwitterion self- and cross-interaction may be the main reason responsible for deviation from ideality, which start at a relatively lower concentration in HEPES as compared to PBS. Indeed, piperazine based molecules and other zwitterionic systems such as arginine are known to form supramolecular assemblies and participate in host-guest complexation reactions [47–49]. We further suspect that this early onset of ion-ion interaction is likely due to the large ionic size of HEPES, which leads to a further decrease in conductivity in an already low conductivity buffer. The average center of mass separation for a pair of HEPES molecules in a 15 mM HEPES solution, calculated assuming uniform and random distribution of all ionic and zwitterionic species, was found to be 5.1 nm or only ~4.8x the diameter of a HEPES molecule. This further supports the possibility of modulation of conductivity by self- and cross-interactions involving anionic and zwitterionic HEPES species.

Next, we tried to fit our experimental data into the theoretical eq. (16) provided by Debye-Hückel-Onsager by combining eq. (16) with $\Lambda_{theo.} = \frac{\kappa}{C_{actual}}$ [35]. One should note here that in eq. (16), $C_{actual}$ is simply the added electrolyte concentration in case of PBS ($= C_{el}$) whereas in HEPES, $C_{actual} = 0.5C_{el}$ (since $[A^-] \approx [HA]$ at pH 7.4 as shown earlier). A plot of $\Lambda_{theo.}$ versus square root of electrolyte concentration gave us the value of $S$ for both PBS and HEPES buffers after linear regression (Fig. 1a and b). The parameter $S$ is essentially a measure of the non-ideality in a system. Its value was found to be nearly 6.5x higher in HEPES than in PBS, which further ascertained that ion-ion interactions are indeed much stronger in HEPES and thus lead to large decrements in its conductivity value.

### 3.2. Comparison of HEPES with other Good's buffers

To verify that the large deviations in conductivity seen in HEPES

**Table 1**
Comparison between ideal and experimentally measured conductivities of PBS buffer at various dilutions.

| PBS buffer at pH 7.4 | Equivalent NaCl concentration (mM) | $\kappa_{expt.}$ (S/m) | $\kappa_{ideal}$ (S/m) | $\Delta\kappa$(S/m) ($\kappa_{ideal} - \kappa_{expt.}$) | % deviation from ideality |
|---|---|---|---|---|---|
| 0.01x | 1.52 | $1.91 \times 10^{-2}$ | $1.91 \times 10^{-2}$ | $-6.00 \times 10^{-5}$ | 0.31% |
| 0.05x | 7.58 | $10.00 \times 10^{-2}$ | $9.57 \times 10^{-2}$ | $-4.30 \times 10^{-3}$ | 4.4% |
| 0.1x | 15.16 | $1.85 \times 10^{-1}$ | $1.91 \times 10^{-1}$ | $1.14 \times 10^{-2}$ | 5.9% |
| 1x | 151.60 | 1.68 | 1.91 | $2.34 \times 10^{-1}$ | 12.2% |

**Table 2**
Comparison between ideal and experimentally measured conductivities of HEPES buffer at various dilutions. The actual electrolyte concentration is 50% of buffer concentration at pH 7.4. Large deviations from ideality were seen even at low electrolyte concentrations.

| HEPES buffer concentration | Actual electrolyte concentration (mM) | $\kappa_{expt.}$(S/m) | $\kappa_{ideal}$ (S/m) | $\Delta\kappa$(S/m) ($\kappa_{ideal} - \kappa_{expt.}$) | % deviation from ideality |
|---|---|---|---|---|---|
| 15 mM at pH 7.4 | 7.5 | $4.78 \times 10^{-2}$ | $5.40 \times 10^{-2}$ | $1.40 \times 10^{-2}$ | 25.9% |
| 30 mM at pH 7.4 | 15.0 | $0.74 \times 10^{-1}$ | $1.08 \times 10^{-1}$ | $3.70 \times 10^{-2}$ | 30.5% |
| 40 mM at pH 7.4 | 20.0 | $0.99 \times 10^{-1}$ | $1.44 \times 10^{-1}$ | $4.40 \times 10^{-2}$ | 30.5% |
| 40 mM at pH 8.5 | 40.0 | $2.02 \times 10^{-2}$ | $2.88 \times 10^{-1}$ | $8.80 \times 10^{-2}$ | 30.5% |

are actually linked to its unique structure and large size, we performed additional experiments to measure the conductivities of a few other Good's buffers (see Table 3) keeping their concentration the same. EPPS (4-(2-hydroxyethyl)-1-piperazinepropanesulfonic acid) was chosen due to its structural similarity with HEPES, varying only by a C–C bond length in its backbone. Similarly, PIPES (1,4-Piperazinediethanesulfonic acid) and POPSO (Piperazine-1,4-bis(2-hydroxy-propanesulfonic acid) dihydrate) also differed from each other by only a single C–C bond length but had two ± charge centers instead of one and a dipole moment quite similar to that of HEPES [50] ($u_{HEPES} = 34.3$ D and $u_{PIPES} = 32.6$ D; see section 5 for details).

When the conductivities of EPPS, PIPES and POPSO were fitted to eq. (16), the $S$ values were found to be very similar to that of HEPES. Any slight deviation in these values as well as those of the absolute conductivities of different buffers were attributed to the disparities in the ion-ion and ion-solvent interactions (also evident from the dissimilar fitted $\Lambda^0$ values in each case), and not so much to the differences in their molecular size, as a slight increase in ionic size does not typically change ionic mobility ($\lambda^0$) significantly. For instance, even though the HEPES anion is approx. 6.5x larger than $Cl^-$, its ionic mobillity is only 3.5x smaller. Overall, the conductivities of HEPES and EPPS were found to be lower than those of PIPES and POPSO leading us to conclude that they may be better buffers for biological impedance measurements, all other factors being the same. Although we have provided experimental evidence which supports this claim, a thorough understanding of the conductivity theory of electrolytes in the presence of neutral dipolar molecules is needed and is not yet established in the literature. Therefore, it is difficult for us to reason out the exact mechanism of conductivity for these systems. One can perhaps perform direct permittivity experiments in the high frequency range (GHz) to validate our claims.

### 3.3. Osmotic pressure on bacterial cells in low electrolyte solutions

After discussing the electrical properties of a good buffering system, we finally focus on the most important aspect, which is the biological functionality of the buffer since the vitality/fitness of any living organism is greatly impacted by the conductivity of its surrounding medium. In this respect, it is intriguing to know how bacteria survive in Good's buffers in spite of their low conductivity. Bacteria have a rigid cell wall that prevents inward/outward flow of ions and maintains a turgor pressure ($\Delta P_0$) across its structure. In addition, the cells have pressure channels that help them actively respond to osmolarity changes in their environment and counter any osmotic stress. The typical value of this turgor pressure is in the range of 2–5 atm [51]. Thus, bacterial cell integrity is maintained through an interplay between the peptidoglycan layers in the cell wall that provide mechanical strength and the mechanosensitive (MS) channels present on the cytoplasmic membrane that allow it to adjust the turgor pressure via active ion transport [52–54]. Under a hypotonic shock condition ($\Delta P > \Delta P_0$), these MS channels open and the bacteria pump out inner ions and metabolites into the medium to maintain osmotic pressure without undergoing lysis.

To understand the role of hypotonicity in low conductivity buffers, we calculated the theoretical suction pressure across bacterial cells, which we defined as ($\Delta P - \Delta P_0$), *i.e.*, the extent of deviation from the turgor pressure. A larger suction pressure implies higher ionic release from the cells into the medium and thus greater stress on them. The osmotic pressure difference between the cells and medium was obtained using the van't Hoff theory for dilute solutions [55], as shown in eq. (19).

$$\Delta P = \Pi_b - \Pi_m = (c_b - c_m)RT \tag{19}$$

where, $\Pi$ is the osmotic pressure and $c$ is the osmolarity of a bacterial cell (denoted by $b$) or the medium (denoted by $m$), $R$ is the gas constant, and $T$ is the absolute temperature. By fixing the bacterial osmolarity at 300 mOsm [56] and the turgor pressure at 4 atm, we estimated the suction pressure for various medium concentrations (or, osmolarities) of PBS and HEPES as shown in Table 4. In addition, the suction pressure for DI water (zero osmolarity) was also calculated as control.

As evident from Table 4, the suction pressure was found to be the highest in DI water followed by 0.01x, 0.05x and 0.1x PBS and 15, 40 and 100 mM HEPES in that order. So next we selected three of these media with similar suction pressures namely DI water, 0.01x PBS and 15 mM HEPES to perform actual cellular ionic release studies. For this, model *S. typhi* bacteria suspended in each of these media were captured on interdigitated microelectrodes using positive dielectrophoresis and their cellular ionic release profiles were measured and plotted as a function of time (Fig. 2a). The dielectrophoretic step was included to enhance the final signal. The results showed a significantly high ionic release in PBS whereas changes were found to be negligible in HEPES and DI water.

The primary reason for the different extent of ionic release in 0.01x PBS and 15 mM HEPES, in spite of very similar suction pressures, was likely linked to the positively charged nitrogen atom in the HEPES molecule that works as an electrostatic crosslinker and stabilizer for the negatively charged bacterial cell wall. This type of crosslinking is not observed in PBS or other standard buffers

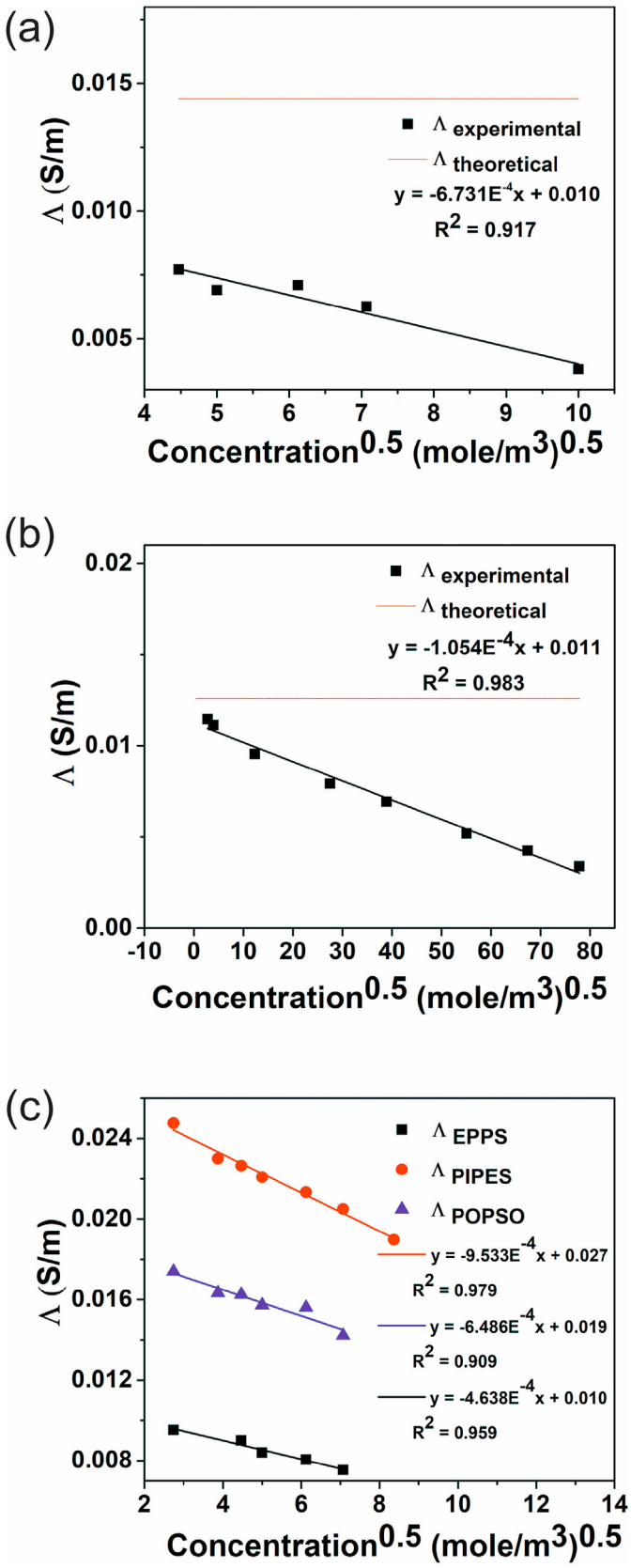


**Fig. 1.** Plot of Λ with $C^{0.5}$ for **(a)** HEPES, **(b)** PBS and **(c)** EPPS, PIPES and POPSO. The slope of the best-fit straight lines yielded the *S* value for HEPES to be nearly 6.5x more than that of PBS, indicating that ion-ion interactions were significantly stronger in HEPES. Similar results were obtained for EPPS, PIPES and POPSO with *S* values 4.4x, 9x and 6x that of PBS, respectively. The horizontal red lines in the top two graphs indicate the theoretically calculated values of ionic mobility ($\Lambda^0$) based on Kohlrausch's law. (For interpretation of the references to colour in this figure legend, the reader is referred to the Web version of this article.)

like tris-HCl [57,58]. This unique crosslinking enhances the stiffness of the cell wall (increase in turgor pressure), allowing cells to remain rigid over higher osmotic pressure differences [59] and thus, leads to lesser ionic release. This in turn makes HEPES a good buffer for bacterial cell studies [33]. The second reason for the difference in ionic release was attributed to the different extents of bacterial cell capture on the electrodes, since dielectrophoretic force depends on the medium conductivity that varies in all the three media (see Table 4). This was, however, ascribed to be a minor reason as the degree of cell capture was not very different in the two media (~28% in HEPES and ~32% in PBS of the total cell population in the bulk). Why was the ionic release higher in 0.01x PBS as compared to DI water is still not fully clear to us. Interestingly, the value of suction pressure was found to be even lower in 40 mM HEPES as compared to 0.05x PBS at pH 7.4, in spite of their matching conductivities (~ 0.1 S/m). This suggested that at a similar conductivity, HEPES is a better medium than PBS because it has lower suction pressure and additional cross-linking property that leads to a less stressful environment for the cells.

Once we established that HEPES provides a more favorable environment for bacterial cells, we conducted further experiments in which ionic release in *S. typhi* and *S. aureus* bacteria was triggered through an active heat treatment process. Cells heated up to 95 °C for 30 min in standard concentrations of PBS, HEPES and EPPS buffers at physiological pH of 7.4 and in DI water showed appreciable cytoplasmic ionic release due to rapid degradation of cellular components and cell lysis, which was measured through impedance spectroscopy (Fig. 2b and c and Fig. S1). Control experiments without heat treatment, on the other hand, did not show any significant impedance change (Fig. S2). Culture data for *S. typhi* confirmed 100% cell death after 30 min of heat treatment, whereas up to 99% cells remained viable after 60 min without any treatment (Fig. S3). Impedance data illustrated that both cell types displayed similar extents of ionic release upon heat treatment (Fig. S4). Also, slightly bigger size IDEs were required to reliably measure impedance response at lower cell concentrations (Fig. S5). Control experiments in which buffer was heated alone did not show any impedance change, indicating that heating did not cause any buffer degradation (data not shown). Among the different media tested, HEPES buffer ($\kappa = 0.04$ S/m) exhibited the best performance followed by EPPS (0.02 S/m) due to a discernibly high signal and high signal to noise ratio (S/N) at the same time. No measurable signals were found in case of 1x PBS (1.6 S/m) especially at lower bacterial cell concentrations suggesting that it is not a good buffer for impedance measurements. On the other hand, the signal measured was highest in DI water but the signal itself suffered from relatively poor S/N. Also, the signals for $10^5$ and $10^6$ cfu/mL overlapped with each other, rendering DI water an unsuitable medium for differentiating bacterial concentrations. These data established that biologically compatible Good's zwitterionic buffers with low ionic conductivity truly have an edge over conventional buffers.

## 4. Conclusions

In summary, we have demonstrated that Good's zwitterionic buffers (*e.g.* HEPES) are a viable and better alternative to the simple buffers (*e.g.* PBS) currently used in the impedance studies of bacterial systems. Zwitterionic solutions have good buffering capacity near the physiological pH and also low conductivity that gives both higher impedance and higher changes in impedance signals. At the

**Table 3**
Conductivity measurements of different zwitterionic buffers at 40 mM and pH = $pKa_2 + 1$ (where all the buffers exist as only anions). The conductivity of PIPES and POPSO was found to be approximately twice as that of HEPES and EPPS due to the presence of two negatively charged sulfide ions per molecule instead of one. The molecular structures were geometrically optimized in Avogadro (s/w version 1.2.0) [66] to calculate their ionic sizes.

| Good's buffer | Chemical structure of the zwitterionic form | $pKa_2$ | Unsolvated anion diameter (A) | $\kappa_{expt.}$ (S/m) |
|---|---|---|---|---|
| 4-(2-hydroxyethyl)-1-piperazineethanesulfonic acid **(HEPES)** | 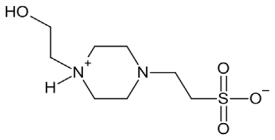 | 7.5 | 10.56 | 0.212 ± 0.011 |
| 4-(2-hydroxyethyl)-1-piperazinepropanesulfonic acid (**EPPS**) | 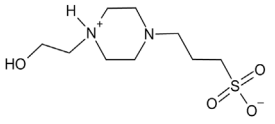 | 8.0 | 10.92 | 0.247 ± 0.025 |
| 1,4-Piperazinediethanesulfonic acid (**PIPES**) | 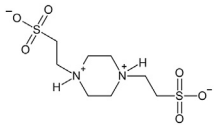 | 6.8 | 12.15 | 0.496 ± 0.025 |
| Piperazine-1,4-bis(2-hydroxy-propanesulfonic acid) dihydrate (**POPSO**) | 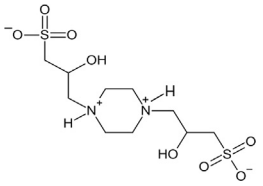 | 7.8 | 13.49 | 0.460 ± 0.006 |

**Table 4**
Theoretical estimate of suction pressure generated on bacterial cells when placed in three different media at various concentrations.

| Buffer | Concentration | $\kappa_{expt.}$ (S/m) | Theoretically calculated medium osmolarity (mOsm) | Suction Pressure ($\Delta P - \Delta P_0$) (atm) |
|---|---|---|---|---|
| HEPES at pH 7.4 | 200 mM | 0.38 | 300.0 | - 4.00 |
| | 100 mM | 0.31 | 150.0 | - 0.28 |
| | 40 mM | 0.10 | 60.0 | 1.92 |
| | 15 mM | 0.04 | 22.5 | 2.83 |
| PBS at pH 7.4 | 1x | 1.60 | 313.0 | - 4.00 |
| | 0.1x | 0.20 | 31.3 | 2.62 |
| | 0.05x | 0.10 | 15.7 | 3.00 |
| | 0.01x | 0.02 | 3.1 | 3.30 |
| DI water (control) | – | $1.00 \times 10^{-4}$ | 0.0 | 3.38 |

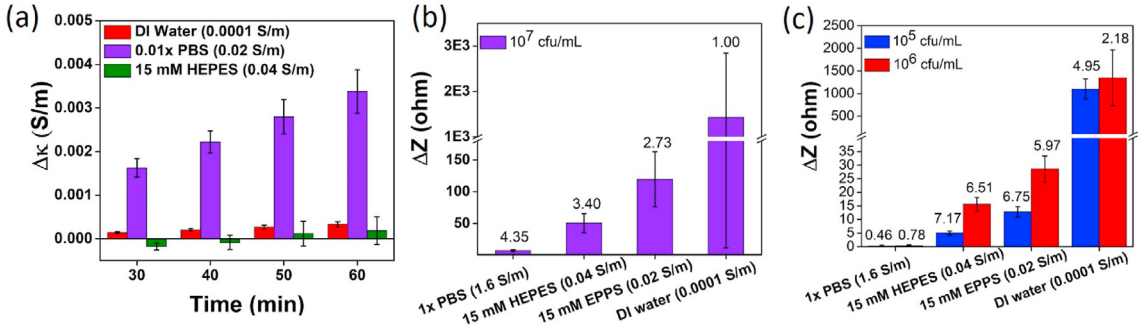


**Fig. 2.** (a) Conductivity change ($\Delta\kappa$, where, $\kappa = \frac{C_c \cos\theta}{|Z|}$ and $\theta$ is the measured impedance phase angle) of the medium due to time-dependent ionic release by *S. typhi* bacteria ($10^7$ cfu/mL) in three different low conductivity media. Similar experiments performed with heat-treated **(b)** *S. typhi* and **(c)** *S. aureus* bacteria in four different standard media (buffer pH was maintained at 7.4). The impedance results plotted after 60 min showed HEPES to have the best performance in terms of simultaneously high signal and high S/N values (given above respective signal bars; see model calculation in SI). Here, the standard deviation has been taken as measure of noise. All the results are plotted at 100 kHz.

same time, cells remain more vital due to the lower suction pressures experienced by them. By comparing HEPES to PBS at the concentrations at which they are typically used in biological studies, we found that 15–20 mM HEPES has significantly lower conductivity than 1x PBS at pH 7.4. This was attributed to HEPES's already low molarity coupled with lower (50%) effective ionic concentration and strong ion-ion interactions mediated by neutral HEPES molecules. Therefore, we conclude that zwitterionic buffers

with large ionic size and lower conductivities are the best for carrying out impedance spectroscopy measurements of bacterial suspensions.

## 5. Methods

### 5.1. Sample preparation

The buffers purchased from Sigma Aldrich (India) were prepared by reconstituting powders/tablets in Milli-Q water of resistivity 18.2 MΩ.cm (Millipore, India), adjusting their pH using 1 M NaOH and filtering them through the sterile nylon filters (13 mm/0.2 μm; Merck, India). Bacterial suspensions were prepared by extracting *Salmonella typhimirium (S. typhi)* and*Staphylococcus aureus* (*S. aureus*) from their exponential growth phase and centrifuging them twice at 10,375 rcf for 10 min each to replace their supernatant with the chosen buffer. The final desired cell concentration was determined using UV−visible spectrophotometry (Shimadzu UV-2600) at 600 nm wavelength.

### 5.2. Impedance measurements

A freshly prepared 20 μL suspension of cells was placed on a clean pair of interdigitated electrodes (IDEs) (50 μm width, 50 μm gap for experiments with *S. typhi* and 100 μm width, 100 μm gap for experiments with *S. aureus*) enclosed in a PDMS chamber (4 mm dia, 1.6 mm thickness) which was covered by a glass cover slip and sealed by vacuum grease. The first impedance reading was taken immediately ($Z_{t=0}$) using an impedance analyzer (E4990A, Keysight) at ± 100 mV and 100 kHz. The cells were then captured at the electrodes for 30 min via positive dielectrophoresis (20 $V_{pp}$, 5 MHz) using a waveform function generator (33500B Agilent). The function generator was switched off and subsequent impedance readings were taken for another 30 min. The final results were plotted as $\Delta\kappa = (\kappa_{t=t} - \kappa_{t=0})$. For heat-induced ionic release measurements, the cell suspensions were heated at 95 °C for 30 min using a water bath and then cooled for another 30 min at room temperature before repeating the impedance measurements as discussed above. The only difference was that no dielectrophoresis was applied in the second set of experiments. The final results were reported as $\Delta Z = (Z_{heat\ treatment\ (t=60)} - Z_{before\ heating\ (t=0)})$. All experiments were performed thrice, and the results were reported as mean ± 1 SD.

### 5.3. Cell culture

Cell viability analysis was performed by withdrawing a 10 μL aliquot from the bacterial suspension ($10^7$ cfu/mL) at any time and spreading it on a sterile Luria-bertani (LB) agar plate (Himedia Labs, India). The plates were placed in a B.O.D. cum shaker incubator at 37 °C for 15−18 h and the bacterial colonies formed were counted the next day. All experiments were performed in triplicate and the results were reported as mean ± 1 SD.

### 5.4. Dipole estimation

The dipole moments of HEPES and PIPES were calculated using density functional theory (DFT) in ORCA package [60]. The geometry in gas phase was optimized using a range-separated, hybrid generalized-gradient approximation (GGA) CAM-B3LYP functional and 6-31G* Pople basis set. Range corrected CAM-B3LYP functional has been shown to be suitable to obtain reliable geometries for conjugated molecules [61,62]. The electronic properties and charge model 5 (CM5) partial atomic charges were calculated at the M06-2X/aug-cc-pVDZ level of theory since the aug-cc-pVDZ basis set that adds diffuse functions to the correlation consistent basis set family has been shown to be appropriate for anions. The dipoles in the gas phase were obtained as $u_{HEPES} = 30.6$ D and $u_{PIPES} = 29.5$ D. The effect of solvent (water) was taken by setting the dielectric constant in the conductor-like polarizable continuum model (C-PCM) to 80.4 [63]. The class IV partial atomic charges were calculated using CM5 [64] on the Multiwfn package [65] yielding $u_{HEPES} = 34.3$ D and $u_{PIPES} = 32.6$ D. The HEPES value was found to be in excellent agreement with experiments on multipole populations for HEPES in crystalline state [50].

## CRediT authorship contribution statement

**Satyam Anand:** Methodology, Investigation, Formal analysis, Writing − original draft, Visualization. **Pragya Swami:** Methodology, Investigation, Formal analysis, Writing − original draft, Visualization. **Gaurav Goel:** Conceptualization, Supervision, Resources, Writing − review & editing, Visualization, Funding acquisition. **Shalini Gupta:** Conceptualization, Supervision, Resources, Writing − review & editing, Visualization, Funding acquisition.

## Declaration of competing interest

The authors declare that they have no known competing financial interests or personal relationships that could have appeared to influence the work reported in this paper.

## Acknowledgements

PS thanks IITD for research fellowship. SG acknowledges IMPRINT (IMP/2018/000236/HT) and DST-Nanomission (SR/NM/NT-1049/2016) grants for funding. We are grateful to Julie Borah for dipole moment calculations of HEPES and PIPES and acknowledge IITD HPC facility for computational resources.

## Appendix A. Supplementary data

Supplementary data to this article can be found online at https://doi.org/10.1016/j.aca.2021.338547.

## References

[1] M. Varshney, Y. Li, Interdigitated array microelectrodes based impedance biosensors for detection of bacterial cells, Biosens. Bioelectron. 24 (2009) 2951−2960, https://doi.org/10.1016/j.bios.2008.10.001.
[2] L. Yang, R. Bashir, Electrical/electrochemical Impedance for Rapid Detection of Foodborne Pathogenic Bacteria, vol. 26, 2008, pp. 135−150, https://doi.org/10.1016/j.biotechadv.2007.10.003.
[3] Y. Xu, X. Xie, Y. Duan, L. Wang, Z. Cheng, J. Cheng, A review of impedance measurements of whole cells, Biosens. Bioelectron. 77 (2016) 824−836, https://doi.org/10.1016/j.bios.2015.10.027.
[4] N. Ramírez, A. Regueiro, O. Arias, R. Contreras, Electrochemical impedance spectroscopy: an effective tool for a fast microbiological diagnosis, Biotecnol. Apl 26 (2006) 72−78.
[5] L. Yang, Electrical Impedance Spectroscopy for Detection of Bacterial Cells in Suspensions Using Interdigitated Microelectrodes, vol. 74, 2008, pp. 1621−1629, https://doi.org/10.1016/j.talanta.2007.10.018.
[6] S.G. Dastider, S. Barizuddin, M. Dweik, M. Almasri, A micromachined impedance biosensor for accurate and rapid detection of E. Coli O157:H7, RSC Adv. 3 (2013) 26297−26306, https://doi.org/10.1039/c3ra44724c.
[7] J. Suehiro, A. Ohtsubo, T. Hatano, M. Hara, Selective detection of bacteria by a dielectrophoretic impedance measurement method using an antibody-immobilized electrode chip, Sensor. Actuator. B Chem. 119 (2006) 319−326, https://doi.org/10.1016/j.snb.2005.12.027.
[8] A. Mortari, A. Adami, L. Lorenzelli, An unconventional approach to impedance microbiology: detection of culture media conductivity variations due to bacteriophage generated lyses of host bacteria, Biosens. Bioelectron. 67 (2015) 615−620, https://doi.org/10.1016/j.bios.2014.09.075.
[9] R. Hamada, H. Takayama, Y. Shonishi, L. Mao, M. Nakano, J. Suehiro, A rapid bacteria detection technique utilizing impedance measurement combined with positive and negative dielectrophoresis, Sensor. Actuator. B Chem. 181 (2013) 439−445, https://doi.org/10.1016/j.snb.2013.02.030.

[10] R. Bashir, Microfluidic biochip for impedance spectroscopy of biological species, Biomed. Microdevices (2001) 201–209.
[11] P.B. Lillehoj, C.W. Kaplan, J. He, W. Shi, C.M. Ho, Rapid, electrical impedance detection of bacterial pathogens using immobilized antimicrobial peptides, J. Lab. Autom. 19 (2014) 42–49, https://doi.org/10.1177/2211068213495207.
[12] R. Gómez, M.R. Ladisch, A.K. Bhunia, R. Bashir, Microfabricated device for impedance-based detection of bacterial metabolism, Mater. Res. Soc. Symp. Proc. 729 (2002) 161–166, https://doi.org/10.1557/proc-729-u4.6.
[13] T. Zhu, Z. Pei, J. Huang, C. Xiong, S. Shi, J. Fang, Detection of bacterial cells by impedance spectra via fluidic electrodes in a microfluidic device, Lab Chip 10 (2010) 1557–1560, https://doi.org/10.1039/b925968f.
[14] N. Couniot, D. Bol, O. Poncelet, L.A. Francis, D. Flandre, A capacitance-to-frequency converter with on-chip passivated microelectrodes for bacteria detection in saline buffers up to 575 MHz, IEEE Trans. Circuits Syst. II Express Briefs. 62 (2015) 159–163, https://doi.org/10.1109/TCSII.2014.2369111.
[15] N. Couniot, A. Afzalian, N. Van Overstraeten-Schlogel, L.A. Francis, D. Flandre, Capacitive biosensing of bacterial cells: sensitivity optimization, IEEE Sensor. J. 16 (2016) 586–595, https://doi.org/10.1109/JSEN.2015.2485120.
[16] S. Bayoudh, A. Othmane, L. Ponsonnet, H. Ben Ouada, Electrical detection and characterization of bacterial adhesion using electrochemical impedance spectroscopy-based flow chamber, Colloids Surfaces A Physicochem. Eng. Asp. 318 (2008) 291–300, https://doi.org/10.1016/j.colsurfa.2008.01.005.
[17] M.A. Mansor, M. Takeuchi, M. Nakajima, Y. Hasegawa, M.R. Ahmad, Electrical impedance spectroscopy for detection of cells in suspensions using microfluidic device with integrated microneedles, Appl. Sci. 7 (2017) 170, https://doi.org/10.3390/app7020170.
[18] N. Couniot, S. Member, A. Afzalian, N. Van Overstraeten-schl, L.A. Francis, Capacitive Biosensing of Bacterial Cells : Sensitivity Optimization, vol. 16, 2015, pp. 1–10, https://doi.org/10.1109/JSEN.2015.2485120.
[19] J. Liu, I. Jasim, A. Abdullah, Z. Shen, L. Zhao, M. El-Dweik, S. Zhang, M. Almasri, An integrated impedance biosensor platform for detection of pathogens in poultry products, Sci. Rep. 8 (2018) 1–10, https://doi.org/10.1038/s41598-018-33972-0.
[20] N. Pal, S. Sharma, S. Gupta, Sensitive and rapid detection of pathogenic bacteria in small volumes using impedance spectroscopy technique, Biosens. Bioelectron. 77 (2016) 270–276, https://doi.org/10.1016/j.bios.2015.09.037.
[21] D. Butler, N. Goel, L. Goodnight, S. Tadigadapa, A. Ebrahimi, Detection of bacterial metabolism in lag-phase using impedance spectroscopy of agar-integrated 3D microelectrodes, Biosens. Bioelectron. 129 (2019) 269–276, https://doi.org/10.1016/j.bios.2018.09.057.
[22] S.G. Dastider, A. Abdullah, I. Jasim, N.S. Yuksek, M. Dweik, M. Almasri, Low concentration E. coli O157:H7 bacteria sensing using microfluidic MEMS biosensor, Rev. Sci. Instrum. 89 (2018) 125009, https://doi.org/10.1063/1.5043424.
[23] J.H. Moore, A. Salahi, C. Honrado, C. Warburton, C.A. Warren, N.S. Swami, Quantifying bacterial spore germination by single-cell impedance cytometry for assessment of host microbiota susceptibility to Clostridioides difficile infection, Biosens. Bioelectron. 166 (2020) 112440, https://doi.org/10.1016/j.bios.2020.112440.
[24] J.S. McGrath, C. Honrado, D. Spencer, B. Horton, H.L. Bridle, H. Morgan, Analysis of parasitic Protozoa at the single-cell level using microfluidic impedance cytometry, Sci. Rep. 7 (2017) 1–11, https://doi.org/10.1038/s41598-017-02715-y.
[25] M.T. Guler, I. Bilican, Capacitive detection of single bacterium from drinking water with a detailed investigation of electrical flow cytometry, Sensors Actuators, A Phys. 269 (2018) 454–463, https://doi.org/10.1016/j.sna.2017.12.008.
[26] M. Goel, A. Verma, S. Gupta, Electric-field driven assembly of live bacterial cell microarrays for rapid phenotypic assessment and cell viability testing, Biosens. Bioelectron. 111 (2018) 159–165, https://doi.org/10.1016/j.bios.2018.04.005.
[27] A.V. Khandelwal, A. Singh, N. Pal, R. Kumar, G. Goel, S. Gupta, AC conductivity measurements of ultradilute colloidal suspensions in HEPES buffer, Langmuir 45 (2019) 14725–14733, https://doi.org/10.1021/acs.langmuir.9b01464.
[28] M. Mallén-Alberdi, N. Vigués, J. Mas, C. Fernández-Sánchez, A. Baldi, Impedance spectral fingerprint of E. coli cells on interdigitated electrodes: a new approach for label free and selective detection, Sens. Bio-Sensing Res. 7 (2016) 100–106, https://doi.org/10.1016/j.sbsr.2016.02.001.
[29] C. Chassagne, E. Dubois, M.L. Jiménez, J.P.M. van der Ploeg, J. van Turnhout, Compensating for electrode polarization in dielectric spectroscopy studies of colloidal suspensions: theoretical assessment of existing methods, Front. Chem. 4 (2016) 30, https://doi.org/10.3389/fchem.2016.00030.
[30] N.E. Good, S. Izawa, Hydrogen ion buffers, Methods Enzymol. 24 (1972) 53–68, https://doi.org/10.1016/0076-6879(72)24054-X.
[31] W.J. Ferguson, K.I. Braunschweiger, W.R. Braunschweiger, J.R. Smith, J.J. McCormick, C.C. Wasmann, N.P. Jarvis, D.H. Bell, N.E. Good, Hydrogen ion buffers for biological research, Anal. Biochem. 104 (1980) 300–310, https://doi.org/10.1016/0003-2697(80)90079-2.
[32] N.E. Good, G.D. Winget, W. Winter, T.N. Connolly, S. Izawa, R.M.M. Singh, Hydrogen ion buffers for biological research, Biochemistry 5 (1966) 467–477, https://doi.org/10.1021/bi00866a011.
[33] P. Swami, A. Sharma, S. Anand, S. Gupta, DEPIS: A combined dielectrophoresis and impedance spectroscopy platform for rapid cell viability and antimicrobial susceptibility analysis, Biosens. Bioelectron. 182 (2021) 113190, https://doi.org/10.1016/j.bios.2021.113190.
[34] A.J. Ballard, C. Dellago, Toward the mechanism of ionic dissociation in water, J. Phys. Chem. B 116 (2012) 13490–13497, https://doi.org/10.1021/jp309300b.
[35] Margaret R. Wright, An Introduction to Aqueous Electrolyte Solutions, Wiley & Sons, 2008, https://doi.org/10.1002/cphc.200800219.
[36] E. Hückel, P. Debye, Zur Theorie der Elektrolyte. I. Gefrierpunktserniedrigung und verwandte Erscheinungen, Phys. Z. 24 (1923) 305, https://doi.org/10.1007/SpringerReference_29987.
[37] L. Onsager, Report on a revision of the conductivity theory, Trans. Faraday Soc. 23 (1927) 341–349, https://doi.org/10.1039/tf9272300341.
[38] R. Ronald, Pethig, Dielectrophoresis: Theory, Methodology and Biological Applications, first ed., John Wiley & Sons, 2017.
[39] J.B. Hasted, D.M. Ritson, C.H. Collie, Dielectric properties of aqueous ionic solutions. Parts I and II, J. Chem. Phys. 16 (1948) 1–21, https://doi.org/10.1063/1.1746645.
[40] M. Taha, I. Khoiroh, M.-J. Lee, Phase behavior and molecular dynamics simulation studies of new aqueous two-phase separation systems induced by HEPES buffer, J. Phys. Chem. B 117 (2013) 563–582, https://doi.org/10.1021/jp305516g.
[41] W.M. Arnold, Positioning and levitation media for the separation of biological cells, in: Conf. Rec. - IAS Annu. Meet. (IEEE Ind. Appl. Soc., 37, 1999, pp. 1468–1475, https://doi.org/10.1109/ias.1999.799187.
[42] P. Atkins, J. De Paula, Physical Chemistry, New York, eighth ed., 2006, https://doi.org/10.1039/c1cs15191f.
[43] B. Ng, P.H. Barry, The measurement of ionic conductivities and mobilities of certain less common organic ions needed for junction potential corrections in electrophysiology, J. Neurosci. Methods 56 (1995) 37–41, https://doi.org/10.1016/0165-0270(94)00087-W.
[44] J. Huang, Confinement induced dilution: electrostatic screening length Anomaly in concentrated electrolytes in confined space, J. Phys. Chem. C 122 (2018) 3428–3433, https://doi.org/10.1021/acs.jpcc.7b11093.
[45] M.A. Gebbie, M. Valtiner, X. Banquy, E.T. Fox, W.A. Henderson, J.N. Israelachvili, Ionic liquids behave as dilute electrolyte solutions, Proc. Natl. Acad. Sci. U.S.A. 110 (2013) 9674–9679, https://doi.org/10.1073/pnas.1307871110.
[46] S. Perkin, Ionic liquids in confined geometries, Phys. Chem. Chem. Phys. 14 (2012) 5052–5062, https://doi.org/10.1039/c2cp23814d.
[47] Z.Y. Chen, M.X. Peng, Supramolecular architectures constructed from piperazine and substituted benzoic acids, J. Chem. Crystallogr. 41 (2011) 137–142, https://doi.org/10.1007/s10870-010-9852-1.
[48] D. Shukla, B.L. Trout, Interaction of arginine with proteins and the mechanism by which it inhibits aggregation, J. Phys. Chem. B 114 (2010) 13426–13438, https://doi.org/10.1021/jp108399g.
[49] A.J. Selinger, D.H. Macartney, Cucurbit[7]uril complexations of Good's buffers, RSC Adv. 7 (2017) 42513–42518, https://doi.org/10.1039/c7ra08865e.
[50] P. Śledzled, R. Kamiński, M. Chruszcz, M.D. Zimmerman, W. Minor, K. Woniak, An experimental charge density of HEPES, Acta Crystallogr. Sect. B Struct. Sci. 66 (2010) 482–492, https://doi.org/10.1107/S0108768110023025.
[51] S. Marion, A. Šiber, Ejecting phage DNA against cellular turgor pressure, Biophys. J. 107 (2014) 1924–1929.
[52] I.R. Booth, M.D. Edwards, S. Black, U. Schumann, S. Miller, Mechanosensitive channels in bacteria: signs of closure? Nat. Rev. Microbiol. 5 (2007) 431–440, https://doi.org/10.1038/nrmicro1659.
[53] Y. Li, P.C. Moe, S. Chandrasekaran, I.R. Booth, P. Blount, Ionic regulation of MSCk, a mechanosensitive channel from Escherichia coli, EMBO J. 21 (2002) 5323–5330, https://doi.org/10.1093/emboj/cdf537.
[54] M. Louhivuori, H.J. Risselada, E. Van Der Giessen, S.J. Marrink, Release of content through mechano-sensitive gates in pressurized liposomes, Proc. Natl. Acad. Sci. U.S.A. 107 (2010) 19856–19860, https://doi.org/10.1073/pnas.1001316107.
[55] J. Van't Hoff, The function of osmotic pressure in the analogy between solutions and gases, Proc. Phys. Soc., London 9 (1887) 307–334, https://doi.org/10.1088/1478-7814/9/1/344.
[56] J.B. Stock, B. Rauch, S. Roseman, Periplasmic space in Salmonella typhimurium and Escherichia coli, J. Biol. Chem. 252 (1977) 7850–7861, https://doi.org/10.1016/S0021-9258(17)41044-1.
[57] Z. Suo, X. Yang, R. Avci, L. Kellerman, D.W. Pascual, M. Fries, A. Steele, HEPES-stabilized encapsulation of Salmonella typhimurium, Langmuir 23 (2007) 1365–1374, https://doi.org/10.1021/la0621721.
[58] M.M. Koerner, L.A. Palacio, J.W. Wright, K.S. Schweitzer, B.D. Ray, H.I. Petrache, Electrodynamics of lipid membrane interactions in the presence of zwitterionic buffers, Biophys. J. 101 (2011) 362–369, https://doi.org/10.1016/j.bpj.2011.05.062.
[59] G. Rani, I. Patri, Importance of being cross-linked for the bacterial cell wall, Phys. Rev. E. 100 (2019) 1–13, https://doi.org/10.1103/PhysRevE.100.062408.
[60] F. Neese, The ORCA program system, Wiley Interdiscip. Rev. Comput. Mol. Sci. 2 (2012) 73–78, https://doi.org/10.1002/wcms.81.
[61] P.A. Limacher, K.V. Mikkelsen, H.P. Lüthi, On the accurate calculation of polarizabilities and second hyperpolarizabilities of polyacetylene oligomer chains using the CAM-B3LYP density functional, J. Chem. Phys. 130 (2009) 194114, https://doi.org/10.1063/1.3139023.
[62] J. Wildman, P. Repiščák, M.J. Paterson, I. Galbraith, General force-field parametrization scheme for molecular dynamics simulations of conjugated materials in solution, J. Chem. Theor. Comput. 12 (2016) 3813–3824, https://doi.org/10.1021/acs.jctc.5b01195.

[63] M. Cossi, N. Rega, G. Scalmani, V. Barone, Energies, structures, and electronic properties of molecules in solution with the C-PCM solvation model, J. Comput. Chem. 24 (2003) 669–681, https://doi.org/10.1002/jcc.10189.
[64] A.V. Marenich, S.V. Jerome, C.J. Cramer, D.G. Truhlar, Charge model 5: an extension of hirshfeld population analysis for the accurate description of molecular interactions in gaseous and condensed phases, J. Chem. Theor. Comput. 8 (2012) 527–541, https://doi.org/10.1021/ct200866d.
[65] T. Lu, F. Chen, Multiwfn: a multifunctional wavefunction analyzer, J. Comput. Chem. 33 (2012) 580–592, https://doi.org/10.1002/jcc.22885.
[66] M.D. Hanwell, D.E. Curtis, D.C. Lonie, T. Vandermeerschd, E. Zurek, G.R. Hutchison, Avogadro: an advanced semantic chemical editor, visualization, and analysis platform, J. Cheminf. 4 (2012) 1–17, https://doi.org/10.1186/1758-2946-4-17.